I&EC research
Industrial & Engineering Chemistry Research
pubs.acs.org/IECR
Article

Low-Temperature Blade-Coated Perovskite Solar Cells

Adriano S. Marques, Roberto M. Faria, Jilian N. Freitas, and Ana F. Nogueira*

Cite This: *Ind. Eng. Chem. Res.* 2021, 60, 7145−7154
Read Online
ACCESS | Metrics & More | Article Recommendations | Supporting Information

ABSTRACT: Spin coating has been the primary choice of deposition method used in the assembly of lab-scale perovskite solar cells. Other deposition methods are still lagging behind, both in terms of device efficiency and in the control of perovskite formation/morphology. Usually, improvements in these processes have been achieved with strategies that are not compatible with the industrial scale, either because of the use of hazardous solvents or due to the costly steps adopted. Here, we report the development of a route to prepare all layers of perovskite solar cells (except the electrodes) through the blade-coating technique, which is a scalable method and can be applied to produce large-area solar cells. We discuss how each process parameter affects the device performance and show that, by tuning the ink composition (i.e., solvent and lead precursors), it is possible to reduce the temperature of the deposition and achieve a perovskite layer with adequate grain size and good coverage of the substrate. With these modifications, a solar cell with a p−i−n configuration assembled in a dry air atmosphere with 15−20% humidity and using the blade coater at 50 °C delivered a maximum of 14.3% of efficiency.

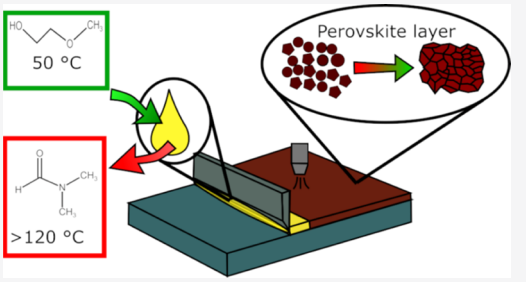

1. INTRODUCTION

Perovskite solar cell (PSC) is a technology expected to revolutionize the renewable energy market in the near future. Yet, these solar cells still present several issues that need to be overcome, some of them related to the fabrication processes, reproducibility, and stability. Spin coating is, by far, the most explored method for the fabrication of PSCs in lab-scale research. However, this method is not suitable for the preparation of large-area devices or in a continuous production flow, which is required to make this photovoltaic technology available in the market. Blade-coating and slot-die are examples of printing methods which are more suitable for industrial-scale production; however, the dynamics of film formation involving perovskite crystallization differ from those observed in the spin-coating method.[1] As a result, part of the knowledge acquired with the use of spin coating over the past years cannot be directly transferred to these methods.

Spin coating working features are very different from the other techniques. The excess material is expelled from the substrate by centrifugal forces and the crystallization of the reminiscent ink is faster because of the high-speed rotation of the substrate, which is in direct contact with the air.[2] In printing methods, there is formation of a wet meniscus that is swept across the substrate, thus forming a wet film. It is the dynamics of the conversion from a wet into a dry film that differs from the spin-coating mechanism. In this case, because of the lack of any external forces acting upon the substrate, the resultant wet film possesses higher solvent content in comparison to that obtained by spin coating. The higher amount of liquid in the wet film reduces the supersaturation process, making the generation of new nucleation sites less favorable, which slows down the crystallization process as a whole and promotes the formation of perovskite films with many imperfections.[3]

To circumvent this situation, several studies have employed different strategies to gain better control over the crystallization process of perovskite films in scalable methods. These strategies include, for example, the use of a vacuum chamber,[2] blowing a dry gas over the substrate,[4] or the use of anti-solvents, in a similar fashion as in the spin-coating process.[5] However, the most adopted strategy is the application of heat during the perovskite deposition.[6,7] Due to the low vapor pressure and high boiling point of the solvents commonly used in perovskite solutions, such as dimethylformamide (DMF), dimethyl sulfoxide, and 1-methyl-2-pyrrolidinone, the temperature required to accelerate evaporation in these cases usually exceeds 130 °C. High temperatures can be harmful to polyethylene terephthalate (PET)-based substrates as they can deform in this condition, making this process unsuitable for flexible PSC.[8]

From an industrial point of view, many of these strategies are not viable either because of the difficulty of implantation (i.e., the need for vacuum chambers) or due to potential environmental and health hazards (i.e., the use of antisolvent bath). Even if these problems were eliminated, the use of high-temperature depositions is energy costly, so other methods are preferred. The sequential two-step deposition method is another

Received: February 24, 2021
Revised: April 20, 2021
Accepted: April 21, 2021
Published: May 3, 2021

https://doi.org/10.1021/acs.iecr.1c00789
Ind. Eng. Chem. Res. 2021, 60, 7145−7154

route that is used.[9] However, this method suffers other problems, such as the incomplete conversion of PbI_2 into perovskite[3] and an additional deposition step in the manufacturing process.

The lack of control in the perovskite crystallization is even more apparent when using the planar configurations (n−i−p or p−i−n).[10] Planar configurations offer a few advantages over the mesoporous configuration: they are simpler and require fewer steps in the manufacturing process. A downside is that it is harder to ensure full coverage of the perovskite layer in this configuration, especially when organic materials are used as the charge collection layers beneath the photoactive layer.[11] Therefore, PSCs in the planar configuration seem to be even more sensitive to the deposition parameters.

The main issues observed during the photoactive layer deposition by printing methods are either related to the lack of control of the perovskite crystallization, which leads to a porous film with pinholes, or by the retraction of the wet film during the evaporation step, leading to regions which are left uncovered, a phenomenon called dewetting.[7] Both problems are related to the dynamics occurring during solvent evaporation. It is clear that control of perovskite layer formation is crucial to obtain efficient PSCs; therefore, studies using scalable methods to produce more efficient devices under mild conditions are of utmost importance.

The power conversion efficiency (PCE) of PSCs made from scalable methods is slowly catching up with PCEs of those obtained with spin coating. A direct comparison between different studies reported in the literature is tricky due to the distinct configurations, cell sizes, and perovskite compositions used in each case. Furthermore, in the majority of the reports dedicated to the development of PSCs by blade-coating, only the perovskite layer is deposited by this scalable method. There are still few works that demonstrate the deposition of all layers using solely scalable methods. Regardless, it is evident from the literature that high PCE can be achieved using some of the beforementioned strategies. For example, 17.3% was obtained by Yang et al.[5] using the anti-solvent method. By changing the perovskite composition and applying high temperature (140 °C), Tang et al.[12] achieved a PCE of 19.3%, a value that is higher than 17.5% displayed by methylammonium iodide perovskite deposited at 150 °C, as demonstrated by Zhong et al.[13] These results demonstrate that PSCs with similar efficiencies to those assembled using spin coating can be obtained when the perovskite layer is prepared by printing methods, keeping the use of spin coating or evaporation for the deposition of the other layers. However, further research in this direction is still necessary to develop processes with fewer restriction parameters and at lower temperatures, to enhance the performance of cells where all of the p−i−n layers are printed. Overall, PCEs of ∼13−15% have been achieved for blade-coating at temperatures higher than 100 °C, with PCEs >17% being achieved for temperatures above 140 °C.

In this work, we demonstrate a route for the preparation of a p−i−n PSC using the blade-coating method for deposition of all layers (except the electrodes). This scalable method allows the observation of conditions that are more representative of the difficulties that will be faced in an industrial production line. The proposed method was based on conditions that would be compatible with an industrial environment (low temperature, single-step deposition) and inverted planar PSC configuration using materials that are already familiar to the organic photovoltaic (OPV) industry. Moreover, DMF was replaced by 2-methoxyethanol[14] as the solvent for the perovskite ink to overcome the problems observed during the deposition step. Herein, we describe the step-by-step process of optimization and the necessary changes introduced to achieve more efficient PSCs prepared by the low-temperature blade-coating routes. The outcome of this work provides a process for deposition of the perovskite layer at 50 °C, which opens up the possibility of application in low energy consumption industrial processes and the use of flexible, plastic substrates.

2. EXPERIMENTAL SECTION

Most of the materials were purchased from Sigma-Aldrich unless stated otherwise. ITO substrates (Delta Technologies, 8−12 Ω/sq) were patterned by photolithography before use. Before the deposition, the substrates were cleaned by sequential sonication in detergent solution, distilled water, acetone, and isopropanol and then submitted to O_2 plasma treatment for 10 min. The deposition of the materials was performed on a ZAA 2300 Zehntner blade coater with a heating mantle placed inside a dry box with humidity control (15−20% relative humidity, dry air atmosphere).

PEDOT:PSS (Clevious) was diluted to a 1:3 ratio in isopropanol to lower the surface energy and improve wettability. The resultant solution was stirred for about an hour and then filtered through a 0.45 μm PTFE filter prior to use. This solution was deposited with a blade height of 30 μm and a blade sweep speed of 15 mm/s at 60 °C. Sequentially, the films were annealed for 10 min at 100 °C.

Perovskite precursors were diluted in the solvent and stirred for 3 h to complete dissolution. With PbI_2 as a lead source, a 1:1 ratio of PbI_2/methylammonium iodide (MAI) was used, while for $Pb(CH_3CO_2)_2{\cdot}3H_2O$ and $PbCl_2$, a molar ratio of 1 Pb^{2+} to 3 MAI was employed to ensure the formation of $CH_3NH_3PbI_3$. The concentration of the ink was varied between 0.50 and 0.20 M, and the relation between the thickness of the final dry film and the concentration of the precursor ink followed a linear pattern. The deposition was carried out under humidity between 10 and 20%, with a blade height of 50 μm and a blade speed of 10 mm/s, and the temperature was adjusted accordingly as described in the text. The dry airflow was suspended over the sample at heights of 5 or 15 cm above the substrate. Annealing of the films was conducted over a heating plate. With PbI_2 as the lead source, the heat treatment was optimized to 100 °C for 1 h, while for compositions containing $Pb(Ac)_2$, this duration could be reduced to just 15 min at the same temperature without loss of performance.

$PC_{61}BM$ (American Dye Source) was dissolved in chlorobenzene at a concentration of 15 mg/mL, and this solution was coated over the perovskite layer with a blade height of 100 μm and a speed of 20 mm/s. After the coating, the substrate was submitted to annealing at 100 °C for 5 min to ensure the removal of the solvent and then transferred to a glovebox, where metallic contacts of calcium (40 nm) and aluminum (70 nm) were deposited by thermal evaporation. The overlap of the deposited layers defined the active area of the solar cells as 0.045 cm^2.

JV scans were performed in an inert atmosphere with a 100 mV/s scan rate using a 2400 Keithley Sourcemeter and an Oriel AAA class simulator with an AM 1.5 G filter as the light source. Statistical distributions were obtained by measuring over 15 different devices in each condition. Veeco Dektak 150 Surface Profiler was used to measure the thickness of the samples. X-ray diffraction (XRD) patterns were obtained on a Rigaku RU200B

https://doi.org/10.1021/acs.iecr.1c00789
Ind. Eng. Chem. Res. 2021, 60, 7145−7154

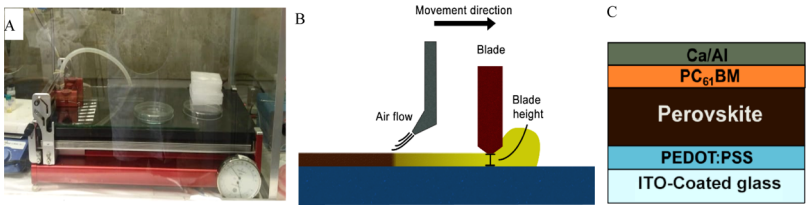

Figure 1. Photograph of the blade-coating system placed inside a dry box; (B) illustration of the deposition process; and (C) configuration of the PSC.

with Cu Kα with a scan rate of 2°/min and operation conditions of 40 kV and 40 mA. Atomic force microscopy (AFM) images were taken in a Nanoscope III from Digital Instruments and UV−vis absorption spectra were obtained in a Hitachi U2900. SEM-FEG images were obtained with a Sigma microscope from Zeiss.

3. RESULTS AND DISCUSSION

All layers deposited by blade-coating were processed at an ambient temperature in a dry air atmosphere and 15−20% of relative humidity, achieved by placing the deposition apparatus inside a box, as displayed in Figure 1A. The development of assembly routes under environmental conditions less controlled than a glovebox ambient is extremely important for an industrial application. The PSCs investigated in this work were assembled in a p−i−n configuration, as illustrated in Figure 1C.

As a hole transport material (HTM), PEDOT:PSS was selected as it is a well-established material in the OPV market. To improve the wettability of the solution and enhance the quality of the film deposited by blade-coating, commercial PEDOT:PSS solution was diluted in isopropanol. After annealing, the deposited film was analyzed with AFM. The images (Figure S1 in the Supporting Information) show that the PEDOT:PSS layer covered the substrate well, without significant defects on the surface. The thickness of this layer was determined with a profilometer to be within the range of 30−40 nm, in agreement with the results from other reports using this type of architecture.[15] Compared to bare ITO, the root-mean-square roughness (R_q) of the substrate estimated through AFM was reduced from 2.84 nm to 1.94 after the deposition of the PEDOT:PSS layer. This value is close to the optimum value (1.84 nm) found by Chen et al.[16] for devices using multication perovskites. Lower roughness values may hinder the subsequent crystallization of perovskite since there are no anchoring points in which perovskite grains can start to grow cohesively.

Next, it was observed that blade-coating the perovskite layer at low temperatures from precursor inks using DMF as the solvent generated needle-like structures (Figure S2 in the Supporting Information), resulting from the slow drying of the solvent.[3,17] To obtain a homogeneous layer, it is imperative to accelerate solvent removal to promote the generation of new nucleation sites. The introduction of a dry air flow briefly after the solution is swept over the substrate (Figure 1B) accelerates the removal of excessive solvent content, partially mimicking the dynamics that occurs inside the spin coater. Although this modification improved the morphology of the film to some extent, the use of precursor inks based on low-vapor-pressure solvents still led to perovskite films with many defects as crystallization forms a 3D network with large voids (Figure S3 in the Supporting Information).

To further accelerate the removal of solvent from the wet film without resourcing to the methods discussed before, the solvent itself must be changed to one with higher vapor pressure. Thus, changing the main solvent in the ink from DMF to 2-methoxyethanol, in association with the use of the air flow, enabled the preparation of a compact perovskite layer. Although 2-methoxyethanol has the ability to coordinate metals, it seems that this solvent is not capable of dissolving PbI_2 by itself, unless MAI is added to the same solution (Figure S4 in the Supporting Information). This feature may also help towards good film formation since a lower interaction between solvent−solute will reach more easily the supersaturation point, favoring the formation of nucleation sites. The AFM and SEM-FEG images of this film (Figure S5 in Supporting Information) prove that the use of 2-methoxyethanol originated a perovskite that is compact, with smaller grains, and completely covers the substrate, without the apparent presence of pinholes.

XRD shows that the as-produced perovskite film deposited from the 2-methoxyethanol-based ink without annealing (blue line in Figure 2) presented the same diffraction pattern observed

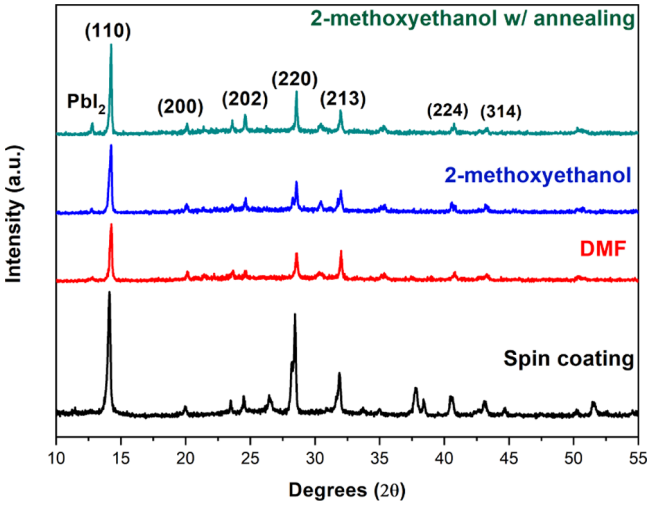

Figure 2. XRD of perovskite films deposited by spin coating or blade-coating using DMF or 2-methoxyethanol (pre- and post-annealing) as the solvent.

for a post-annealed perovskite film deposited through the standard spin coating and from blade-coating using a DMF-based ink. In the case of 2-methoxyethanol, the perovskite crystallization is almost completed during the deposition process. Then, during annealing, the diffraction peaks become more intense and better defined (narrower full width half maximum), indicating higher crystallinity after this process. The diffractograms of Figure 2 also show that the resultant perovskite layer is composed of polycrystalline grains, without a preferred orientation. For the blade-coated films, a small diffraction peak at 12.7°, related to the (001) diffraction plane of hexagonal PbI_2, can be seen. This indicates that a residual amount of PbI_2 was formed during the deposition and, during the annealing process,

https://doi.org/10.1021/acs.iecr.1c00789
Ind. Eng. Chem. Res. 2021, 60, 7145−7154

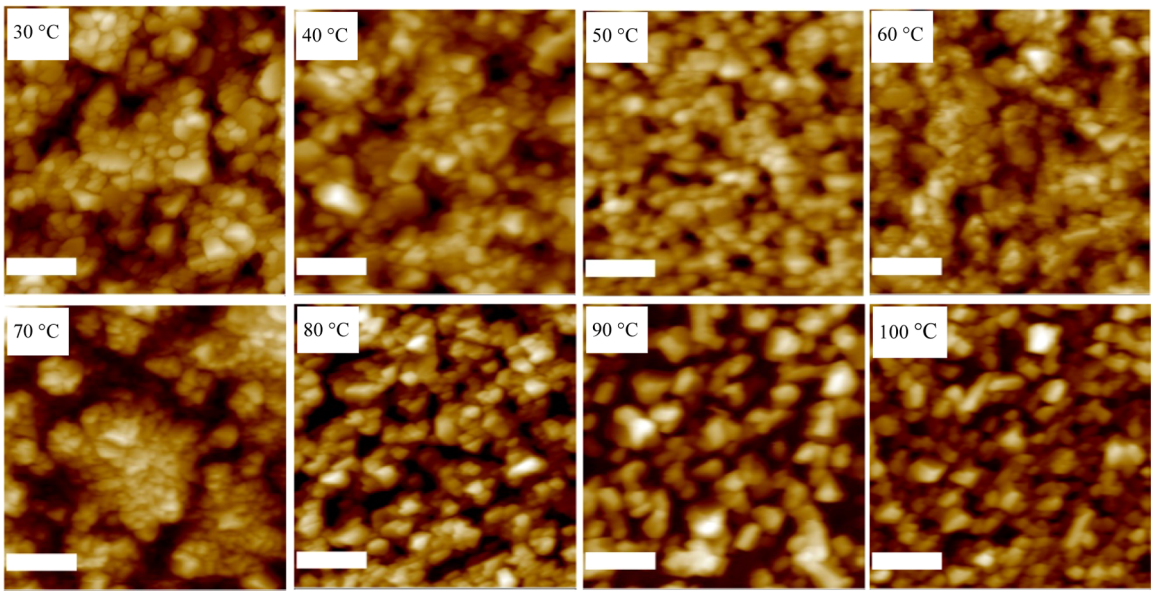

Figure 3. AFM images of perovskite layers deposited at varying temperatures from the 2-methoxyethanol ink. The scale bar represents 500 nm.

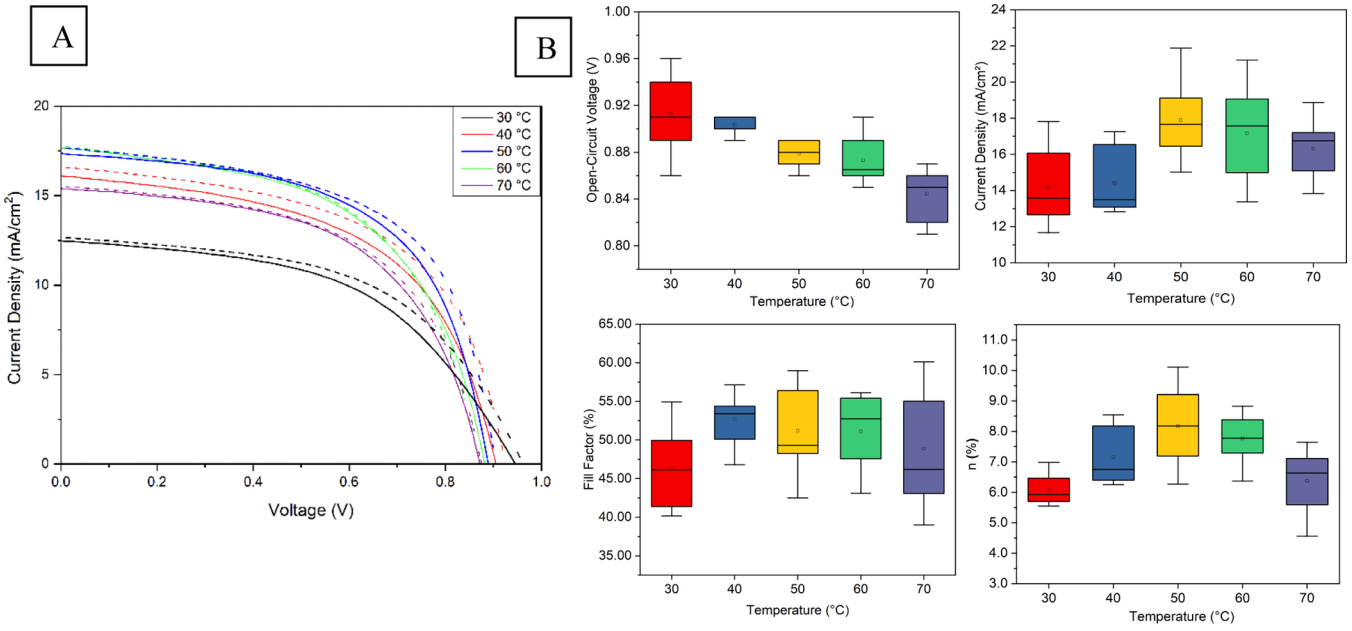

Figure 4. (A) JV curves of the best device in each condition, where the temperature was varied. The dashed lines are the forward scan. (B) Statistical distribution of the photovoltaic parameters obtained in each condition.

this formation is further increased. The presence of small quantities of PbI_2 in the device is not necessarily harmful, and there are reports showing that it might even increase the final performance of the solar cell.[18]

To continue the assembly of the cell, $PC_{61}BM$ was used as electron transport material (ETM) (Figure 1C) and deposited via blade-coating as well. $PC_{61}BM$ was selected for the same reason as PEDOT:PSS, that is, this material is successfully used in OPV devices, even for depositions in large areas.[19] The $PC_{61}BM$ film was analyzed with AFM and SEM-FEG (Figure S6 in the Supporting Information), and the images showed that the fullerene layer follows the pattern of the layer underneath. In the perovskite layer obtained from the DMF ink, $PC_{61}BM$ could not fully cover the substrate due to the voids present in the perovskite. For the film prepared from the 2-methoxyethanol ink, $PC_{61}BM$ showed full coverage of the layer underneath and originated a smooth layer without defects. The thickness of the fullerene layer was estimated using the profilometer and ranged between 50 and 60 nm.

The photovoltaic devices containing the perovskite deposited from the DMF ink delivered a poor-performing device, with PCE around 3.7%. Surprisingly, the devices prepared from 2-methoxyethanol had an even lower performance than those with DMF, even though the AFM and SEM-FEG images showed that a perovskite layer with fewer imperfections was obtained. By fine-tuning the concentration of the 2-methoxyethanol ink, the performance of the cells was increased and an inverse correlation between the perovskite film thickness (from 280 to 160 nm) and the PCE was found, achieving up to 6.39% for the thinner film (Figure S9 and Table S1 in the Supporting Information). An

https://doi.org/10.1021/acs.iecr.1c00789
Ind. Eng. Chem. Res. 2021, 60, 7145−7154

increase in the short-circuit current (J_{sc}), fill factor (FF), and open-circuit voltage (V_{oc}) was observed and resulted from the improvement of both series and shunt resistances, as a consequence of a better collection of the photogenerated charges related to the size of the grains generated from the more volatile solvent. We attribute this trend to the fact that the perovskite layer obtained from the 2-methoxyethanol ink and blade-coating process comprises smaller grains in comparison to those prepared by spin-coating processes. According to Correa-Baena et al.,[20] a perovskite layer composed of small crystals has an increased surface area and consequently more surface defects. In this case, for a given thickness length, the photogenerated charges have to travel across a larger number of grains to reach the ETM or HTM, increasing the probability of recombination, thus reducing the performance of the device in comparison to films with larger grain sizes.

In an effort to surpass the performance limitation imposed by the small grains obtained by this method and achieve higher efficiency, the effect of the temperature applied during the deposition of perovskite was investigated but always keeping it below 100 °C in order to develop a low-temperature process. AFM images (Figure 3) show that the morphology of the perovskite film slightly changes upon variation of temperature. Overall, the application of heat during the deposition allowed the perovskite to grow into larger grains, and the distribution of grain area became broader (see the histogram in Figure S10 in the Supporting Information). In a more detailed analysis, two different regimes are evident: one from ambient temperature up to 60 °C and one above 70 °C. The former generates perovskite grains that have shared borders with neighbor grains, forming a continuous layer. At lower temperatures, the surface is rougher. As temperature rises, the layer seems to become more homogeneous, reaching a turning point at 60 °C. Beyond this temperature, the perovskite shows a different behavior: the agglomerates become more spaced and larger voids start to appear, which can be related to the presence of pinholes, making the surface heterogeneous again. This trend is also observed in lower-magnification images (Figure S11 in the Supporting Information) and by the superficial roughness analysis; R_q was estimated to be 19.1, 18.1, 11.8, 13.0, and 20.6 nm for films deposited at 30, 40, 50, 60, and 70 °C, respectively. Lower surface roughness is expected to improve the interface between the perovskite and the ETM if the film is also continuous and free from pinholes.

Solar cells containing the perovskite deposited at different temperatures were assembled and characterized. The JV curves (Figure 4 and Table 1) show that within the range of 30−50 °C, the PCE increased with the temperature, reaching a maximum at 50 °C, followed by a slight decrease at 60 °C. From 40 up to 60 °C, there is a large increase in the current density generated by the devices, which is related to a reduction in the series resistance. The V_{oc} presented a different trend, being inversely proportional to the increase in temperature. A drop in V_{oc} is often associated with an increase in the recombination process, especially in the perovskite layer with open grain boundaries.[21] Comparing the AFM images with low and high magnification in the range of 30−50 °C, as the temperature rises, more black spots appear in the perovskite surface, which were associated with the presence of pinholes. In temperatures higher than 60 °C, the films show larger defects and the V_{oc} values decrease even further. The V_{oc} of devices prepared at 70 °C show the highest variance observed in the statistical analysis (Figure 4B and Table S2 in the Supporting Information), suggesting that the drop in this parameter might be associated with the recombination due to the existence of more defects in this perovskite film. The PCE increased up to 50 °C, and from this point on, it decays due to the reduction of V_{oc} and FF, mainly affected by the low quality of the perovskite film obtained at higher temperatures. The drop in performance above 50 °C was unexpected since an increase in efficiency is usually observed when the perovskite grains become larger. Considering these results, applying a temperature of 50 °C during the deposition seems to be the best compromise between the photovoltaic parameters, leading to the highest PCE.

Until 60 °C, the rise of temperature had little influence on the thickness of the resultant films, which was around 160 nm. At temperatures above 70 °C, the drying dynamics of the perovskite film is different, and the wet film converts into dry before the gas flow reaches the substrate. The uncontrollable crystallization process led to the formation of films with large pinholes, as observed in the AFM images. This condition also led to more translucid films (Figure S12 in the Supporting Information) due to their lower thickness, which was as low as 100 nm at 100 °C. Considering these features, solar cells with perovskite films deposited in conditions above 70 °C were not assembled. Along with the temperature modification, other experimental parameter that was explored was a change in the height of the gas flow outlet in relation to the sample. A farther position from the surface of the sample (15 cm) negatively impacts the performance of the device because the influence of the flow becomes weaker. Consequently, the perovskite crystals grow less cohesively, with many grains separated from the others, without sharing corners (Figure S13 in the Supporting Information). The photovoltaic performance of devices prepared in this condition displayed an intermediary performance compared to the ones previously studied, with J_{sc} around 14.6 mA/cm^2 and V_{oc} of only 0.86 V (Table S3 and Figure S14 in the Supporting Information).

We also investigated how the lead source in the ink could influence the performance of the device by replacing PbI_2 with $PbCl_2$ and lead acetate ($Pb(Ac)_2$) while keeping 2-methoxyethanol as the solvent. All previous parameters that gave rise to better performance were kept unchanged (i.e., temperature of 50 °C and a 5 cm distance from the airflow to the sample). With this change, it is possible to achieve better control of the crystallization and film formation as each precursor plays a distinct role in this mixed ink composition. $Pb(Ac)_2$ promotes the formation of a smooth, dense perovskite layer without defects, and the acetate ion can react with the exceeding methylammonium, generating CH_3NH_3Ac, which is easily removed from the sample, accelerating the crystal growth during film formation.[22,23] $PbCl_2$ role is to enhance the crystal formation and promote the growth of the perovskite grains due to the presence of chlorine ions.[24,25] This composition generates

Table 1. JV parameters of the best device at each deposition temperature.

condition (°C)	V_{oc} (V)	J_{sc} (mA/cm^2)	FF (%)	η (%)	R_s (Ω cm^2)	R_{sh} (Ω cm^2)
30	0.96	12.66	53.04	6.46	17.27	526.50
40	0.93	16.59	55.61	8.54	7.30	408.90
50	0.91	17.67	58.34	9.33	6.08	450.35
60	0.87	17.77	55.38	8.57	7.76	354.82
70	0.88	15.54	55.73	7.58	7.78	519.12

https://doi.org/10.1021/acs.iecr.1c00789
Ind. Eng. Chem. Res. 2021, 60, 7145−7154

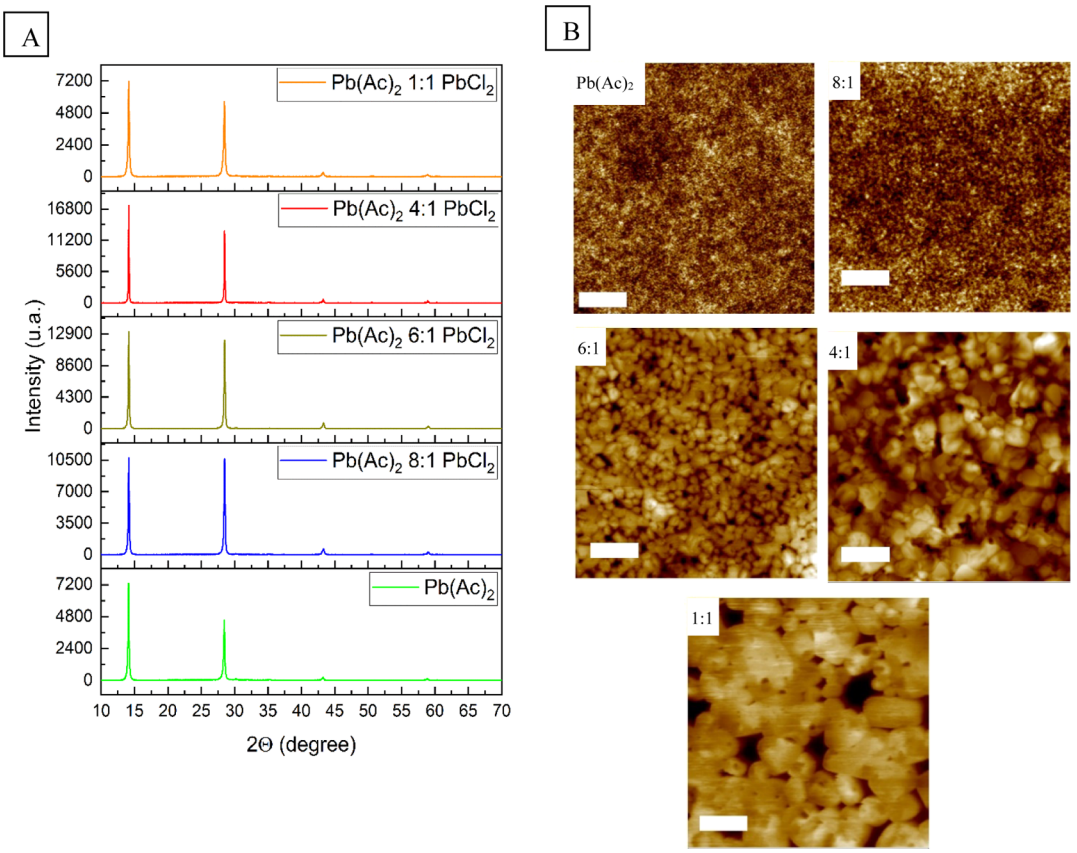

Figure 5. XRD and (B) AFM images of perovskite films obtained from inks with mixed compositions. Scale bars represent 2 μm.

the $CH_3NH_3PbI_{3-x}Cl_x$ perovskite, which has a long carrier diffusion that can go up to 1 μm.[25]

In mixed ink compositions, the ratio between the precursors is another parameter that has to be adjusted to obtain the best working condition. Here, the $Pb(Ac)_2/PbCl_2$ ratio was altered from 1:0 to 1:1 to investigate the effect of the change in the formulation. The previously optimized deposition parameters (temperature of 50 °C and 5 cm distance of the airflow in relation to the sample) were kept unchanged. As observed with the PbI_2 precursor, the dissolution of the starting materials in 2-methoxyethanol occurred only after MAI was added in the solution, especially in the compositions containing larger amounts of $PbCl_2$. Differently from the traditional method employing PbI_2, when using other precursors, it was necessary to use a 3:1 ratio of MAI/Pb to achieve the necessary iodide concentration in the final product. Compared to the previous depositions using PbI_2 as the lead source, we observed that the transition from the wet yellow film to the dark brown perovskite was less abrupt with these mixed compositions, especially with higher ratios of $Pb(Ac)_2$. A video of the deposition process can be seen in the Supporting Information.

The XRD of the films prepared from these mixed inks (Figure 5A) is slightly different from those displayed in Figure 2. The main difference is the intensity of the peaks at 14.1, 28.5, and 43.3° regarding the baseline related to the (110), (220), and (330) planes, respectively. This indicates that the perovskite crystals are highly oriented with the long axis parallel to the substrate.[26] These high-oriented crystals occur both with a mixed precursor solution and with pure $Pb(Ac)_2$, suggesting that this effect is not due to the $CH_3NH_3PbI_{3-x}Cl_x$ composition but might be related to the use of lead acetate as the precursor, although other reports have achieved a similar result using $PbCl_2$ and DMF,[4] with a little formation of $CH_3NH_3PbCl_3$ in that case, which is absent here.

The addition of Cl^- in the precursor solution increases the crystallinity of the resultant perovskite, as can be seen by the enhancement of the diffraction peaks in films with crescent content of $PbCl_2$. At the 4:1 $Pb(Ac)_2/PbCl_2$ ratio, the diffraction peaks reach a maximum and then decrease upon further addition of Cl^-, eventually reaching similar values of the film prepared only with $Pb(Ac)_2$. Moreover, films with higher contents of $PbCl_2$ (1:1 ratio) seem to suffer from a degradation mechanism: the as-deposited films looked just like the others containing $Pb(Ac)_2$, but shortly after annealing, these films changed from shiny reflexive dark brown perovskite to a hazy dark gray film. This behavior seems to be related to the crystals continuously growing during the heat treatment, eventually forming a rough perovskite layer, which explains the hazy gray aspect. The massive crystal growth during the annealing also generates mechanical stress that induces the formation of cracks in the film.[22] If these films were kept in an annealing treatment, eventually they would massively deteriorate (photo available in Figure S15 in the Supporting Information).

The films obtained from each ink composition were also analyzed with AFM (Figure 5B). From the images, it is evident that the morphology of the layer prepared from pure $Pb(Ac)_2$ ink is vastly different from those obtained using PbI_2 (Figure 3), with smaller and less-defined grains. The small grain size achieved in this composition is due to the ability of $Pb(Ac)_2$ to rapidly generate crystallization nuclei. It also contributes to achieving high coverage of the substrate as there was no sign of pinholes within this film. Upon addition of $PbCl_2$ into the ink,

https://doi.org/10.1021/acs.iecr.1c00789
Ind. Eng. Chem. Res. 2021, 60, 7145−7154

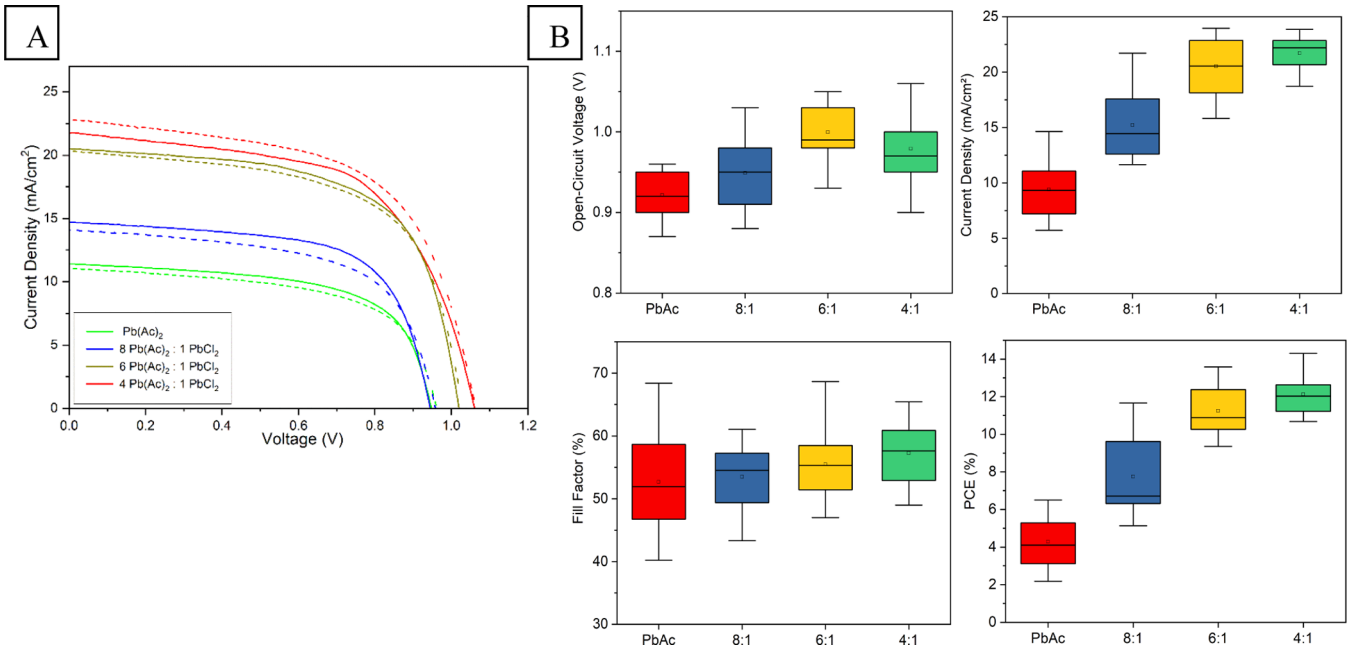

Figure 6. (A) JV curves of the best device in each condition, where the ink composition (ratio) was varied. The dashed lines are the forward scans. (B) Statistical distribution of the photovoltaic parameters obtained in each condition.

the perovskite begins to grow mostly because of the presence of Cl^- in the solution. At 8:1 ratio, the area of the grains is only slightly smaller than that obtained from pure PbI_2 in 2-methoxyethanol, although, in the mixed composition, the grains seem more cohesive, sharing their boundaries with adjacent grains, generating a compact layer, as can be seen in higher magnification images (Figure S16 in the Supporting Information). Precursor inks with 6:1 and 4:1 ratios generated a perovskite layer with vastly superior grain sizes while maintaining the cohesive aspect between the grains. However, higher proportions of Cl^- in the ink (1:1 ratio) led to the formation of films containing many defects. As can be seen in AFM images, the film with this composition has grains larger than 2 μm, as well as smaller grains in the sub-micron range. With this heterogeneity, the coverage of the substrate is impaired and large defects are visible in the active layer. Moreover, because of the deterioration that this composition undergoes during annealing, it was not possible to measure the photovoltaic performance of most of the devices prepared from this ink. Of the few that we could measure, the photovoltaic performance was very poor, with a substantial drop in V_{oc} and FF (Figure S15 in the Supporting Information).

Solar cells were assembled using the films prepared from the precursor solutions containing $Pb(Ac)_2$ and $PbCl_2$ and the optimum deposition conditions previously developed for the PbI_2 ink using 2-methoxyethanol as the solvent. JV curves are displayed in Figure 6. With these precursors, the active layer was slightly thicker, around 250 nm. The change of precursor also allowed a reduction of the annealing time to just 15 min due to the formation and easy removal of CH_3NH_3Ac from the film.

The addition of a small amount of $PbCl_2$ in the precursor solution (8:1 $Pb(Ac)_2/PbCl_2$ ratio) introduced a few changes in the morphology of the perovskite film, which reflected in the photovoltaic performance, resulting in an increase of J_{sc} and V_{oc}. Devices containing higher $PbCl_2$ ratios (6:1 and 4:1) showed a large improvement in their performance compared to all previous conditions investigated, as can be seen in Table 2.

Table 2. JV Parameters of the Best Device in Each Condition

mix ratio	V_{oc} (V)	J_{sc} (mA/cm^2)	FF (%)	PCE (%)	R_s (Ω cm^2)	R_{sh} (Ω cm^2)
$Pb(Ac)_2$	0.95	11.42	61.80	6.69	6.95	658.23
8:1	0.96	14.08	60.56	8.17	6.51	638.65
6:1	1.03	20.51	62.61	13.09	5.08	505.91
4:1	1.06	22.86	58.82	14.30	6.48	335.07

While FF remained nearly constant for all compositions, the V_{oc} was well above average (ca. 0.90 V) for devices using PEDOT:PSS as HTM. Reports in the literature state that the small amount of chlorine present in this kind of perovskite is not enough to change the highest energy occupied molecular orbital and lowest unoccupied molecular orbital of the material and that both $CH_3NH_3PbI_3$ and $CH_3NH_3PbI_{3-x}Cl_x$ have nearly identical absorption spectra.[27] Thus, the observed enhancement of V_{oc} may be explained by these films having lower electron−hole recombination.[28] The smaller chlorine content in 8:1 was not enough to exhibit the same behavior observed in 6:1 and 4:1 ratios, as can be seen by the difference in the V_{oc} (Table 2). The 6:1 and 4:1 ratios allowed a great improvement in the quality of the material, as observed by their higher crystallinity in the DRX compared to other compositions, as well as in the perovskite grain size. The current density followed the observed trend for these grain sizes, highlighting how this feature is important for the performance of the device.

The 6:1 and 4:1 ratios were the compositions that resulted in PSCs with the higher efficiencies. Statistically, many of the photovoltaic parameters were similar between these two conditions, although the 4:1 ratio led to a slightly higher and narrower J_{sc} distribution, which resulted in a higher PCE. The champion cell using the 4:1 $Pb(Ac)_2/PbCl_2$ composition achieved a J_{sc} of 22.86 mA/cm^2 and a V_{oc} of 1.06 V, resulting in a PCE of 14.30%. This result is above the other reports that used blade-coating or slot die with a similar cell structure that achieved between 10 and 13% efficiency,[6,29,30] with the

https://doi.org/10.1021/acs.iecr.1c00789
Ind. Eng. Chem. Res. 2021, 60, 7145−7154

advantage of using low temperature for the deposition of perovskite.

The solvent modification is another pivotal point that we have explored in this work. To further demonstrate the impact of 2-methoxyethanol as a solvent, a perovskite ink with a 4:1 $Pb(Ac)_2/PbCl_2$ ratio was prepared in DMF and used to deposit perovskite layers following the most optimized parameters previously described (Figure S19 in the Supporting Information). AFM images show that the resulting perovskite film is composed of elongated grains and has many pinholes, similar to the one obtained with PbI_2 in DMF. The best PCE achieved was around 6.0%, which is higher than the one previously obtained using PbI_2 in DMF. This outcome is largely due to the higher current density, a consequence of the better charge transport of the perovskite containing chlorine, but this result is still much lower than that obtained with 2-methoxyethanol.

In summary, in this work, we presented the steps adopted in the development of an accessible, low-temperature route for the preparation of PSCs using a scalable method. The set of parameters investigated here, comprising tuning of the lead source and use of a more volatile solvent in the precursor ink associated with the gas flow and low temperature during the blade-coating deposition of the perovskite layer were all crucial for achieving higher PCEs. The results obtained with a combination of lead chloride and lead acetate revealed that the small grain size was the main reason for the low performance of the devices prepared from PbI_2. The formation of small grains seems to be a counterpart of this type of deposition at mild conditions. The solvent has a major role in allowing the deposition to happen at low temperatures since it must evaporate quickly so the super saturation of the wet film can occur and generate numerous nucleation sites, which will then lead to full coverage of the substrate. However, once the process has started, the growth of these new crystals is unfavorable, which means that, to obtain good results, the use of solvents with high vapor pressure must be combined with materials, such as $PbCl_2$, that enhance the crystal growth, as discussed here. Other materials described in the literature such as $Pb(SCN)_2$[31] and NH_4Cl[32] may have the same effect and result in good performing devices as well.

It should be noted that the development of a route for blade-coating the perovskite layer at temperatures as low as 50 °C leading to reasonable PCEs has a strong appeal for industrial applications due to the reduced energy demand and lower cost. This versatile method could be extended for a variety of applications. For example, it could be employed for the assembly of flexible solar cells, where transparent plastic substrates such as PET, polyethylene naphthalate, polycarbonate, and polyimide could be used. Furthermore, blade-coating has been one of the techniques explored for the assembly of monolithic perovskite/silicon tandem solar cells using polished silicon wafers or texture silicon with pyramids less than 1 μm in height.[33] For this kind of application, the low-temperature blade-coating process developed here is also advantageous to preserve the integrity of silicon and other lower-lying layers and interfaces in the tandem device.

4. CONCLUSIONS

In this work, we presented a systematic investigation for the development and optimization of a route to produce PSCs with the premise of using blade-coating deposition under mild conditions, with procedures that could be applied in industrial environments. Adaptations to the process had to be made to achieve a condition within those requirements that also allowed the formation of a perovskite layer with large grains and full coverage, that could deliver a good device performance. The commonly used DMF is not a suitable choice as a solvent for perovskite ink for blade-coating deposition in low-temperature conditions. Changing the solvent to 2-methoxyethanol allowed the deposition at 50 °C, and a preliminary optimization of the photoactive layer allowed to increase the efficiency up to 9.3%. To further enhance the performance, it was necessary to change the lead precursor in the ink from lead iodide to a combination of lead chloride and lead acetate. Then, by fine-tuning the ink composition, it was possible to achieve a condition to obtain the advantages from both materials, leading to a perovskite with large-grain size and with good coverage of the substrate. The optimized process led to a p−i−n photovoltaic device with 14.3% efficiency, in which all layers (except the electrodes) were prepared by blade-coating at low temperatures. The process developed here could be used for the assembly of flexible cells on plastic substrates and also for the assembly of monolithic perovskite/silicon tandem cells, where the use of low temperatures is crucial to avoid damages to the other components of the devices.

■ ASSOCIATED CONTENT

Supporting Information

The Supporting Information is available free of charge at https://pubs.acs.org/doi/10.1021/acs.iecr.1c00789.

AFM images of the ITO substrate, PEDOT:PSS and PCBM layers, and perovskite films deposited at different conditions (varied ink composition, temperature, or gas outlet position); histograms of grain area estimated from AFM images; FEG-SEM images of perovskite films deposited at different conditions; photographs of perovskite inks and perovskite films; UV−vis of perovskite films deposited at different temperatures; and JV curves (forward and reverse scans) and photovoltaic parameters of cells containing perovskite layers prepared from different ink compositions (solvent and Pb precursor), with different film thicknesses, or different gas outlet positions during the blade coating deposition (PDF)

Blade-coating deposition of the perovskite layer (MP4)

■ AUTHOR INFORMATION

Corresponding Author

Ana F. Nogueira − *Laboratório de Nanotecnologia e Energia Solar, Chemistry Institute, University of Campinas—UNICAMP, 13083-970 Campinas, São Paulo, Brazil;* orcid.org/0000-0002-0838-7962; Email: anafla@unicamp.br

Authors

Adriano S. Marques − *Laboratório de Nanotecnologia e Energia Solar, Chemistry Institute, University of Campinas—UNICAMP, 13083-970 Campinas, São Paulo, Brazil*

Roberto M. Faria − *Institute of Physics, University of São Paulo, 13560-970 São Carlos, São Paulo, Brazil;* orcid.org/0000-0002-0088-442X

Jilian N. Freitas − *Center for Information Technology Renato Archer—CTI, 13069-901 Campinas, São Paulo, Brazil*

Complete contact information is available at: https://pubs.acs.org/10.1021/acs.iecr.1c00789

Notes

The authors declare no competing financial interest.

■ ACKNOWLEDGMENTS

The authors would like to thank the funding agencies Conselho Nacional de Desenvolvimento Científico e Tecnológico—CNPq (grant 140392/2015-7), São Paulo Research Foundation (FAPESP, grant 2017/12582-5), INEO, and Capes for the financial support. A.F.N. and J.N.F. gratefully acknowledge the support from the FAPESP (grant 2017/11986-5) and Shell and the strategic importance of the support given by ANP (Brazil's National Oil, Natural Gas and Biofuels Agency) through the R&D levy regulation.

■ REFERENCES

(1) Howard, I. A.; Abzieher, T.; Hossain, I. M.; Eggers, H.; Schackmar, F.; Ternes, S.; Richards, B. S.; Lemmer, U.; Paetzold, U. W. Coated and Printed Perovskites for Photovoltaic Applications. *Adv. Mater.* **2019**, *31*, 1806702.

(2) Parvazian, E.; Abdollah-zadeh, A.; Akbari, H. R.; Taghavinia, N. Fabrication of perovskite solar cells based on vacuum-assisted linear meniscus printing of MAPbI3. *Sol. Energy Mater. Sol. Cells* **2019**, *191*, 148−156.

(3) Remeika, M.; Qi, Y. Scalable solution coating of the absorber for perovskite solar cells. *J. Energy Chem.* **2018**, *27*, 1101−1110.

(4) Su, J.; Cai, H.; Ye, X.; Zhou, X.; Yang, J.; Wang, D.; Ni, J.; Li, J.; Zhang, J. Efficient Perovskite Solar Cells Prepared by Hot Air Blowing to Ultrasonic Spraying in Ambient Air. *ACS Appl. Mater. Interfaces* **2019**, *11*, 10689−10696.

(5) Yang, M.; Li, Z.; Reese, M. O.; Reid, O. G.; Kim, D. H.; Siol, S.; Klein, T. R.; Yan, Y.; Berry, J. J.; van Hest, B. F. A. M.; Zhu, K. Perovskite ink with wide processing window for scalable high-efficiency solar cells,". *Nat. Energy* **2017**, *2*, 17038.

(6) Deng, Y.; Peng, E.; Shao, Y.; Xiao, Z.; Dong, Q.; Huang, J. Scalable fabrication of efficient organolead trihalide perovskite solar cells with doctor-bladed. *Energy Environ. Sci.* **2015**, *8*, 1544−1550.

(7) Dai, X.; Deng, Y.; Van Brackle, C. H.; Huang, J. Meniscus fabrication of halide perovskite thin films at high throughput for large area and low-cost solar panels. *Int. J. Extreme Manuf.* **2019**, *1*, 022004.

(8) Zardetto, V.; Brown, T. M.; Reale, A.; Di Carlo, A. Substrates for flexible electronics: A practical investigation on the electrical, film flexibility, optical, temperature, and solvent resistance properties. *J. Polym. Sci., Part B: Polym. Phys.* **2011**, *49*, 638−648.

(9) Kim, Y. Y.; Park, E. Y.; Yang, T.-Y.; Noh, J. H.; Shin, T. J.; Jeon, N. J.; Seo, J. Fast two-step deposition of perovskite via mediator extraction treatment for large-area, high-performance perovskite solar cells. *J. Mater. Chem. A* **2018**, *6*, 12447−12454.

(10) Wu, W.-Q.; Chen, D.; Caruso, R. A.; Cheng, Y.-B. Recent progress in hybrid perovskite solar cells based on n-type materials. *J. Mater. Chem. A* **2017**, *5*, 10092−10109.

(11) Lee, J.; Kang, H.; Kim, G.; Back, H.; Kim, J.; Hong, S.; Park, B.; Lee, E.; Lee, K. Achieving Large-Area Planar Perovskite Solar Cells by Introducing an Interfacial Compatibilizer. *Adv. Mater.* **2017**, *29*, 1606363.

(12) Tang, S.; Deng, Y.; Zheng, X.; Bai, Y.; Fang, Y.; Dong, Q.; Wei, H.; Huang, J. Composition Engineering in Doctor-Blading of Perovskite Solar Cells. *Adv. Energy Mater.* **2017**, *7*, 1700302.

(13) Zhong, Y.; Munir, R.; Li, J.; Tang, M.-C.; Niazi, M. R.; Zhao, K.; Amassian, A. Blade-Coated Organolead Triiodide Perovskite Solar Cells with Efficiency > 17%: An In Situ Investigation. *ACS Energy Lett.* **2018**, *3*, 1078−1085.

(14) Hendriks, K. H.; van Franeker, J. J.; Bruijnaers, B. J.; Anta, J. A.; Wienk, M. M.; Janssen, R. A. J. 2-Methoxyethanol as a new solvent for processing methylammonium lead halide perovskite solar cells. *J. Mater. Chem. A* **2017**, *5*, 2346−2354.

(15) Yang, Z.; Chueh, C.-C.; Zuo, F.; Kim, J. H.; Liang, P.-W.; Jen, A. K.-Y. High-Performance Fully Printable Perovskite Solar Cells via Blade-Coating Technique under the Ambient Condition. *Adv. Energy Mater.* **2015**, *5*, 1500328.

(16) Chen, C.-C.; Chang, S. H.; Chen, L.-C.; Kao, F.-S.; Cheng, H.-M.; Yeh, S.-C.; Chen, C.-T.; Wu, W.-T.; Tseng, Z.-L.; Chuang, C. L.; Wu, C.-G. Improving the efficiency of inverted mixed-organic-cation perovskite absorber based photovoltaics by tailing the surface roughness of PEDOT: PSS thin film. *Sol. Energy* **2016**, *134*, 445−451.

(17) Jung, Y.-S.; Hwang, K.; Heo, Y.-J.; Kim, J.-E.; Lee, D.; Lee, C.-H.; Joh, H.-I.; Yeo, J.-S.; Kim, D.-Y. One-Step Printable Perovskite Films Fabricated under Ambient Conditions for Efficient and Reproducible Solar Cells. *ACS Appl. Mater. Interfaces* **2017**, *9*, 27832−27838.

(18) Jacobsson, T. J.; Correa-Baena, J.-P.; Halvani Anaraki, E.; Philippe, B.; Stranks, S. D.; Bouduban, M. E. F.; Tress, W.; Schenk, K.; Teuscher, J.; Moser, J.-E.; Rensmo, H.; Hagfeldt, A. Unreacted PbI_2 as a Double-Edged Sword for Enhancing the Performance of Perovskite Solar Cells. *J. Am. Chem. Soc.* **2016**, *138*, 10331−10343.

(19) Zhang, K.; Chen, Z.; Armin, A.; Dong, S.; Xia, R.; Yip, H. L.; Shoaee, S.; Huang, F.; Cao, Y. Efficient Large Area Organic Solar Cells Processed by Blade-Coating With Single-Component Green Solvent. *Sol. RRL* **2018**, *2*, 1700169.

(20) Correa-Baena, J.-P.; Anaya, M.; Lozano, G.; Tress, W.; Domanski, K.; Saliba, M.; Matsui, T.; Jacobsson, T. J.; Calvo, M. E.; Abate, A.; Grätzel, M.; Míguez, H.; Hagfeldt, A. Unbroken Perovskite: Interplay of Morphology, Electro-optical Properties, and Ionic Movement. *Adv. Mater.* **2016**, *28*, 5031−5037.

(21) Sherkar, T. S.; Momblona, C.; Gil-Escrig, L.; Ávila, J.; Sessolo, M.; Bolink, H. J.; Koster, L. J. A. Recombination in Perovskite Solar Cells: Significance of Grain Boundaries, Interface Traps, and Defect Ions. *ACS Energy Lett.* **2017**, *2*, 1214−1222.

(22) Qiu, W.; Merckx, T.; Jaysankar, M.; Masse de la Huerta, C.; Rakocevic, L.; Zhang, W.; Paetzold, U. W.; Gehlhaar, R.; Froyen, L.; Poortmans, J.; Cheyns, D.; Snaith, H. J.; Heremans, P. Pinhole-free perovskite films for efficient solar modules. *Energy Environ. Sci.* **2016**, *9*, 484−489.

(23) Zhang, W.; Saliba, M.; Moore, D. T.; Pathak, S. K.; Hörantner, M. T.; Stergiopoulos, T.; Stranks, S. D.; eperon, G. E.; Alexaner-Webber, J. A.; Abate, A.; Sadhanala, A.; Yao, S.; Chen, Y.; Friend, R. H.; Estroff, L. A.; Wiesner, U.; Snaith, H. J. Ultrasmooth organic-inorganic perovskite thin-film formation and crystallization for efficient planar heterojunction solar cells. *Nat. Commun.* **2015**, *6*, 6142.

(24) Liang, P.-W.; Liao, C.-Y.; Chueh, C.-C.; Zuo, F.; Williams, S. T.; Xin, X.-K.; Lin, J.; Jen, A. K.-Y. Additive enhanced crystallization of solution-processed perovskite for highly efficient planar-heterojunction solar cells. *Adv. Mater.* **2014**, *26*, 3748−3754.

(25) Stranks, S. D.; Eperon, G. E.; Grancini, G.; Menelaou, C.; Alcocer, M. J. P.; Leijtens, T.; Herz, L. M.; Petrozza, A.; Snaith, H. J. Electron-Hole Diffusion Lengths Exceeding 1 Micrometer in an Organometal Trihalide Perovskite Absorber. *Science* **2013**, *342*, 341−344.

(26) Docampo, P.; Hanusch, F. C.; Giesbrecht, N.; Angloher, P.; Ivanova, A.; Bein, T. Influence of the orientation of methylammonium lead iodide perovskite crystals on solar cell performance. *APL Mater.* **2014**, *2*, 081508.

(27) Chen, Q.; Zhou, H.; Fang, Y.; Ztieg, A. Z.; Song, T.-B.; Wang, H.-H.; Xu, X.; Liu, Y.; Lu, S.; You, J.; Sun, P.; Mckay, J.; Goorsky, M. S.; Yang, Y. The optoelectronic role of chlorine in $CH_3NH_3PbI_3$ (Cl)-based perovskite solar cells. *Nat. Commun.* **2015**, *6*, 7269.

(28) Liu, J.; Prezhdo, O. V. Chlorine Doping Reduces Electron-Hole Recombination in Lead Iodide Perovskites: Time-Domain Ab Initio Analysis. *J. Phys. Chem. Lett.* **2015**, *6*, 4463−4469.

(29) Wang, D.; Zheng, J.; Wang, X.; Gao, J.; Kong, W.; Cheng, C.; Xu, B. Improvement on the performance of perovskite solar cells by doctor-blade coating under ambient condition with hole-transporting material optimization. *J. Energy Chem.* **2019**, *38*, 207−213.

(30) Peng, Y.; Cheng, Y.; Wang, C.; Zhang, C.; Xia, H.; Huang, K.; Tong, S.; Hao, X.; Yang, J. Fully doctor-bladed planar heterojunction perovskite solar cells under ambient condition. *Org. Electron.* **2018**, *58*, 153−158.

https://doi.org/10.1021/acs.iecr.1c00789
Ind. Eng. Chem. Res. 2021, 60, 7145−7154

(31) Ke, W.; Xiao, C.; Wang, C.; Saparov, B.; duan, H.-S.; Zhao, D.; Xiao, Z.; Schulz, P.; Harvey, S. P.; Liao, W.; Meng, W.; Yu, Y.; Cimaroli, A. J.; Jiang, C.-S.; Zhu, K.; Al-Jassim, M.; Fang, G.; Mitzi, D. B.; Yan, Y. Employing Lead Thiocyanate Additive to Reduce the Hysteresis and Boost the Fill Factor of Planar Perovskite Solar Cells. *Adv. Mater.* **2016**, *28*, 5214−5221.

(32) Chen, Y.; Zhao, Y.; Liang, Z. Non-thermal annealing fabrication of efficient planar perovskite solar cells with inclusion of NH_4Cl. *Chem. Mater.* **2015**, *27*, 1448−1451.

(33) Chen, B.; Yu, Z. J.; Manzoor, S.; Wang, S.; Weigand, W.; Yu, Z.; Yang, G.; Ni, Z.; Dai, X.; Holman, Z. C.; Huang, J. Blade-coated Perovskite on Textured Silicon for 26%-Efficient Monolithic Perrovskite/Silicon Tandem Solar Cells. *Joule* **2020**, *4*, 850−864.

https://doi.org/10.1021/acs.iecr.1c00789
Ind. Eng. Chem. Res. 2021, 60, 7145−7154